1

OVERVIEW OF AFM

1.1 THE ESSENCE OF THE TECHNIQUE

Atomic force microscopy or AFM is a method to see the shape of a surface in three-dimensional (3D) detail down to the nanometer scale [1,2]. AFM can image all materials—hard or soft, synthetic or natural (including biological structures such as cells and biomolecules)—irrespective of opaqueness or conductivity. The sample is usually imaged in air, but can be in liquid environments and in some cases under vacuum. The surface morphology is not perceived in the usual way, that is, by line-of-sight, reflections, or shadows.[1] Rather, at each point or pixel within a 2D array over the surface, a measurement of *surface height* is made using a sharp solid force probe. One could thus say that AFM is "blind microscopy"; it essentially uses touch to image a surface, unlike light or electron microscopes. The force probe may move over a stationary sample or remain stationary as the sample is moved under the probe, as discussed in Chapter 4. Typically, one chooses to display the height measurements as colors or tints, some variant of dark-is-low/bright-is-high, with a gradient of color or grayscale in between. Thus, an *image of surface topography* is obtained for viewing purposes, as exemplified in Figure 1.1, for several surfaces relevant to hard and soft materials science, nanotechnology, and biology. The typical range of these measurements is several micrometers vertically with

[1] Or, as with scanning electron microscopy, by secondary electron emission enhanced or suppressed to give the perception of reflections and shadows.

Atomic Force Microscopy: Understanding Basic Modes and Advanced Applications, First Edition.
Greg Haugstad.

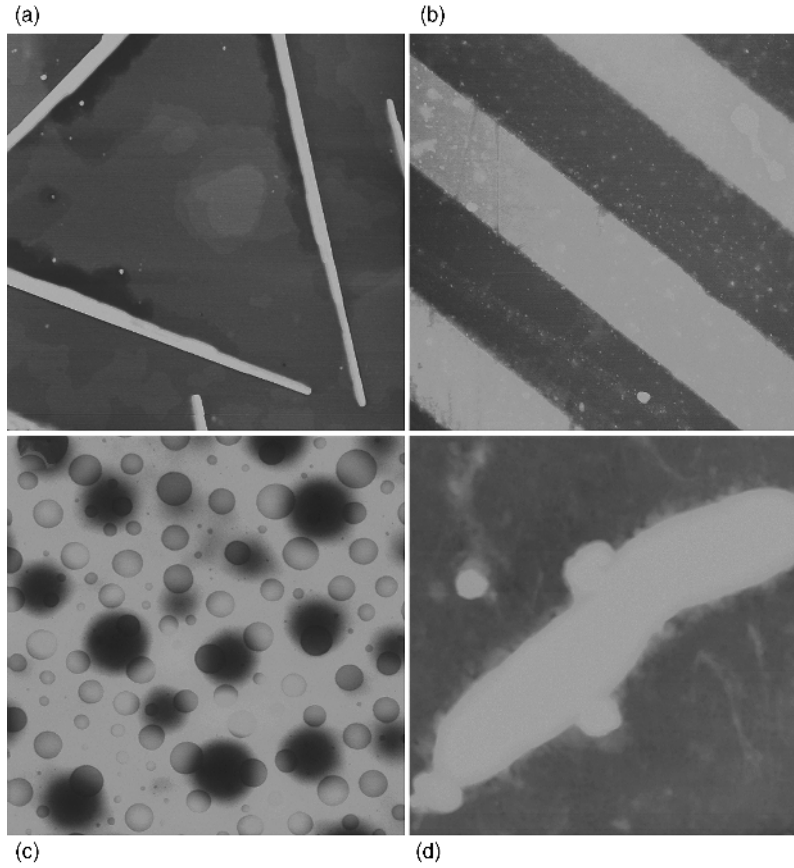

FIGURE 1.1 In-air surface topography images of (a) silver rods (15-nm tall) grown from a AgBr(111) surface by photoreduction, 5×5 μm [3]; (b) gold and aluminum lines (∼50-nm tall) lithographically created on silicon, 25×25 μm; (c) surface of a ∼1-μm thick polymer film (deepest valleys ∼100 nm) of a 75:25 blend of butyl and lauryl methacrylates (spin coated onto a silicon wafer), 8×8 μm; (d) wastewater bacterium (170-nm tall) on filtration membrane, 3×3 μm [4].

subnanometer height resolution and several tens of micrometers laterally, ranging up to ∼100 μm, with a highest lateral resolution of ∼1 nm (when not limited by the pixel density of the image, i.e., physical resolution as opposed to digital resolution).

Given that the image is constructed from height numbers, one also can measure *peak-to-valley* distances, compute *standard deviations* of height, compile the *distribution* of heights or slopes of hills . . . , and even *Fourier-analyze* a surface to identify *periodic* components (ripples or lattices) or dominant length scales (akin to a scattering technique). These *metrics* of topography can be relevant to technological performance or biological function, whether in microelectronics (e.g., roughness of layers or grain size, in deposition processes), tribology (e.g., friction and wear on hard disk read heads), polymer–drug coatings (e.g., surface contour area impacting

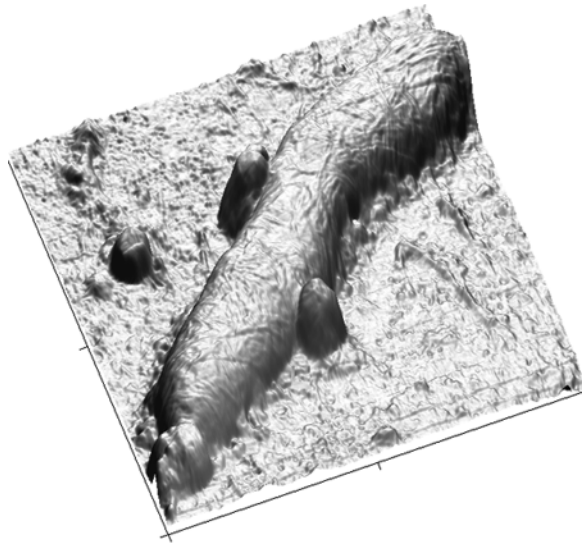

FIGURE 1.2 Wastewater bacterium (170-nm tall) on filtration membrane, 3×3 μm.

drug release rate), intrabody medical devices (e.g., shape of surface in contact with cells, tissues), cellular membranes and surface components (e.g., phospholipid bilayer, protein receptors), and much more.

As a bonus, with real height numbers in hand, one can render images in 3D perspective. The example in Figure 1.2 is an image of the dividing bacterium rendered in 2D in Figure 1.1d. *Computer-simulated light reflections and shadows* are incorporated to give the sense of a macroscale object and to enhance the perception of texture, even though the features may be nanoscale (i.e., below the resolution of real light microscopes). The angle of simulated illumination as well as the angle of "view" can be adjusted. The vertical scale has been exaggerated; the height of the bacterium is 180 nm, but is made to appear almost twice that high in comparison to the lateral scale. This is typical; often 3D-rendered AFM images exaggerate height by an even greater factor to bring out features for viewing.[2]

A bacterium, or for that matter anything hundreds of nanometers tall, is in fact a large object for AFM. With AFM's high precision, one can measure molecular or atomic crystal structures and indeed image striking, meandering steps. Figure 1.3 contains an image of five terraces on a surface of single crystal $SrTiO_3$, in ambient air. The steps between terraces comprise a "staircase" of increasing brightness from top right to bottom left. Also shown is a *histogram* representation or *population* of heights in the image: the number of pixels counted within narrow increments or "bins" of height (further discussed in Chapter 4), with the height scale increasing from left to right. One sees five well-resolved histogram peaks, spaced by 4 Å

[2] There is nothing wrong with this type of presentation, provided the scaling is made known to the viewer.

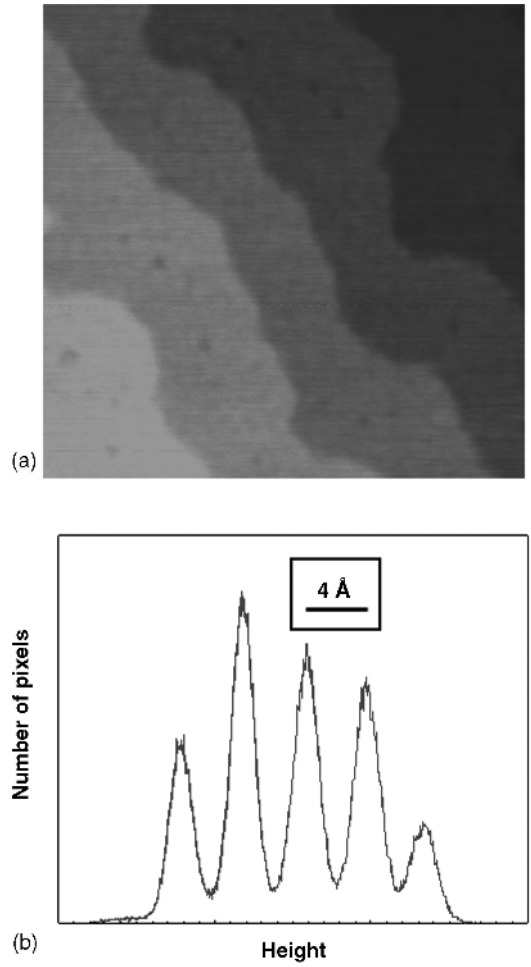

FIGURE 1.3 (a) 800×800-nm height image of $SrTiO_3(100)$. (b) Histogram of preceding image.

between adjacent peaks, the signature step size between adjacent (100) planes of $SrTiO_3$. The area under each peak—the total count of pixels—quantifies the relative surface area of each terrace within the imaged region. The shapes of step contours and extent of terraces are interesting for many reasons; for example, these may provide information on the *kinetics* and *thermodynamics* by which steps and terraces form during material growth processes [5].

How exactly does AFM determine the local height of a surface? By touching it with a sharp object, while measuring the *vertical or "Z" displacement* needed to do so. This "touching," however, can be very subtle; that is, the metaphor can be taken too literally. Moreover, heights are *indirectly* measured, as detailed in Chapter 4. In

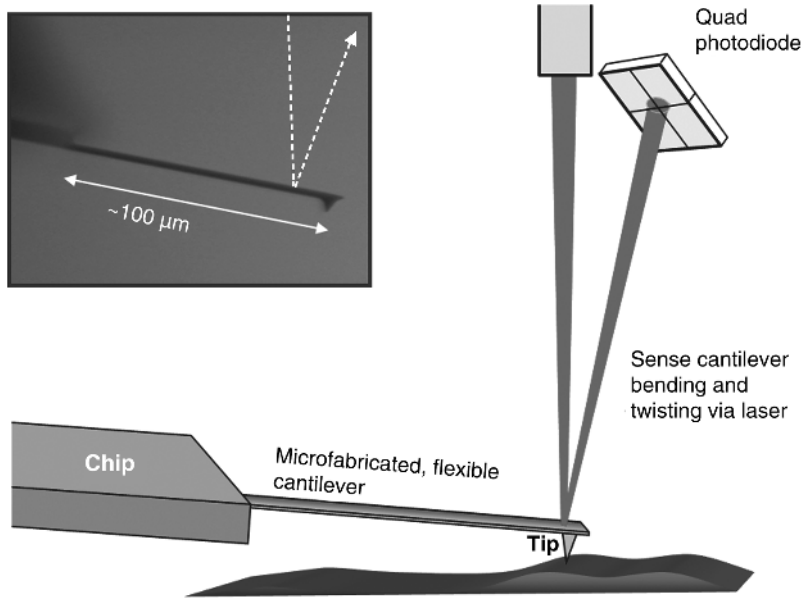

FIGURE 1.4 Schematic illustration of the core components of AFM: tip/cantilever/chip, focused laser beam, quad photodiode. Inset is light micrograph of a real AFM cantilever/tip viewed from the side; cantilever is 100 μm long, tip 10 μm tall.

most AFM designs,[3] and as depicted in Figure 1.4, the sharp *tip* (also known as stylus, probe, or needle) is attached to a flexible *microcantilever*—essentially a microscopic diving board—which bends under the influence of force. The behavior is that of a tip attached to a spring; a cantilever bent upward or downward is that of a compressed or extended spring. The bending is usually measured by reflecting a laser beam off of the cantilever and onto a split photodiode (a horizontal "knife edge"), the output of which gauges the position of the laser spot. The vertical tip movement, in turn, is quantified from this cantilever bending. Lateral forces that torque the tip, causing the cantilever to twist, can be measured via the horizontal movement of the laser spot (at a vertical "knife edge"). (We discuss lateral force methods in detail in Chapter 7.) The measurement typically will handle a vertical tip range of hundreds of nanometers, and with subnanometer resolution as detailed in Chapter 3 (including caveats). The vertical spring constants of cantilevers in common use range from 10^{-2} N/m to 10^{2} N/m (or nN/nm), resulting in a measurable force range from pico-Newtons to micro-Newtons.

In the simplest picture, one would bring the tip into contact with a surface, start moving or *scanning* laterally, and measure the vertical tip movement as the

[3] Several force measurement schemes are treated in Ref. [2], including the original method of Binnig et al. in Ref. [1].

cantilever bends up and down to gauge surface height while the tip slides over the surface. (Imagine the surface moving back and forth in Figure 1.4.) By doing so, over a 2D grid of locations across the surface, one could build up a surface *topograph*: height versus *X* and *Y*. But this scheme generally does not work very well because the up and down bending of the cantilever corresponds to higher and lower spring forces pressing the tip against the surface such that the tip or sample might be damaged due to high contact force atop the hills, and, conversely, the tip and sample might separate or *disengage* in the deepest valleys. Moreover, there is always some arbitrary *tilt* between a sample surface and the *X*–*Y* plane of the scanning device such that forces would continually grow while scanning in one direction (cantilever bending further up) and the surface would "recede from view" if scanning far in the opposite direction as contact is lost. The range of the split photodiode measurement may not be sufficient to gauge large excursions of the tip up or down anyway (i.e., large laser spot excursions). So AFMs normally employ scanning devices that displace not only *X* and *Y* but also *Z*, via *feedback*, to offset variations in height and keep the pressing force approximately constant.[4] This *reactive Z displacement* is, then, the sought measurement of surface height.[5] We will discuss in greater detail each of these components—tip/cantilever, laser, photodetector, scanner, and feedback circuit—as well as nonidealities and caveats associated with these components, plus the physics of the tip–sample interaction that affect topographic imaging—in Chapters 2–5.

1.2 PROPERTY SENSITIVE IMAGING: VERTICAL TOUCHING AND SLIDING FRICTION

AFM is, however, much more powerful as an analytical tool! One is touching the surface of an object that one wishes to understand. Using touch to measure height, but nothing else, seems unambitious. We all know that a piece of upholstery feels different from a piece of concrete. Food has a different texture if moist instead of dry. We wish to detect, even quantify, such differences with AFM. After all, a major goal of microscopy is to *differentiate* objects or regions. This may include materials such as metals, semiconductors, ceramics, minerals, polymers, or other organics—or biological entities such as cells, tissues, and biomolecules (e.g., proteins, polysaccharides, nucleic acids, lipids)—or, for that matter, may differentiate synthetic from biological. Also, one wishes to detect *changes* in a given material—say from *amorphous*, meaning atomically disordered, to *crystalline*—or from biologically *functional* to *denatured.* If we can touch at the nanoscale, and in a highly controlled way . . . , cannot we distinguish materials or biological entities based on unique

[4] This force is measured as the fixed vertical displacement of the tip, relative to its position when the cantilever is unbent as seen in Section 1.5, times the spring constant of the cantilever. The latter is approximately specified by the manufacturer or measured by the user as described in Section 3.7 and Appendix 1.

[5] Even this displacement is not directly measured, as detailed in Chapter 4.

properties, that is, how they "feel?" Understanding surface topography measurements by AFM is a first goal, but much of this book's subject matter relates to this second question: how to differentiate sample constituents and measure the properties of a given constituent. This encompasses changes in properties under variable environments including gaseous, liquid, and variable temperature, upon chemical treatment or with aging, and as a function of measurement parameters such as rate or applied force [6–8].

A common property metric is the rigidity or *stiffness* of a material, sensed as the resistance to the tip pushing in—the increase of *repulsive* force per unit distance of deformation.[6,7] *Rubbery* polymers, for example, derive their soft character from molecular composition, with further dependence on temperature and absorbed small molecules, such as water, residual solvent, or other such *plasticizers*, that tend to soften the material. Small changes in chemical structure or environmental parameters, such as temperature or humidity, can lead to dramatic changes in material properties. These properties are not only manifest in the 3D deformation of the sample as the tip pushes in but also at the *interface* between tip and sample. In what sense? AFM is exquisitely sensitive to the "grab" exerted by one material on another when we try to pull them apart or slide one past the other. The resistance to these motions depends in part on the strength of *attractive forces* between the materials constituting tip and sample. Most materials, when touching or very close together ($\sim$1 nm), experience *dipole–dipole* forces that produce *attraction*; in special cases in liquids, they produce *repulsion*. (This is discussed in Chapter 2.) Resistance to separation or sliding also can depend on *molecular motions* at the interface or internal to the sample. How? The motion of the tip itself can *activate* molecular motion or produce a stress that decreases the barrier to *thermal activation* of molecular motions at ambient conditions [9]. Once the tip and the excited molecules are far apart, there is no way for this motional energy to be given back to the tip. It is lost or *dissipated* as "heat" into the sample, in the most general sense of the term, meaning a large number of atomic and molecular *degrees of freedom* (e.g., bond vibrations); this heat, in turn, dissipates into the environment. Of course, these atoms and molecules already had motional energy prior to tip interaction; but in their "collisions" with the tip, this energy has on average increased. This is analogous to the kinetic energy of a car imparted to air (primarily N_2) molecules while driving down the road. Some molecules may actually collide with the back of the car to aid its motion, but on average the ensemble of collisions takes away kinetic energy (is dissipative for the car).

Thus, due to the "grab" exerted on the tip as manifest in adhesion and friction, as well as the finite mechanical stiffness of the sample, we have three differentiating measurements at our disposal. Figure 1.5 schematically depicts the raw

[6] This can be calibrated given that force is measurable as stated above and distance of deformation can be determined in comparison with force–distances measurements on a rigid reference sample; see Chapter 3.

[7] This is not to be confused with hardness, which formally refers instead to a resistance to mechanical yield, meaning plastic deformation, such as the creation of a permanent indent or hole. Some use stiffness and hardness interchangeably, but formally this is incorrect, just as using stiffness and density interchangeably would be incorrect. See Johnson, K.L., *Contact Mechanics*. 1985, New York: Cambridge University Press.

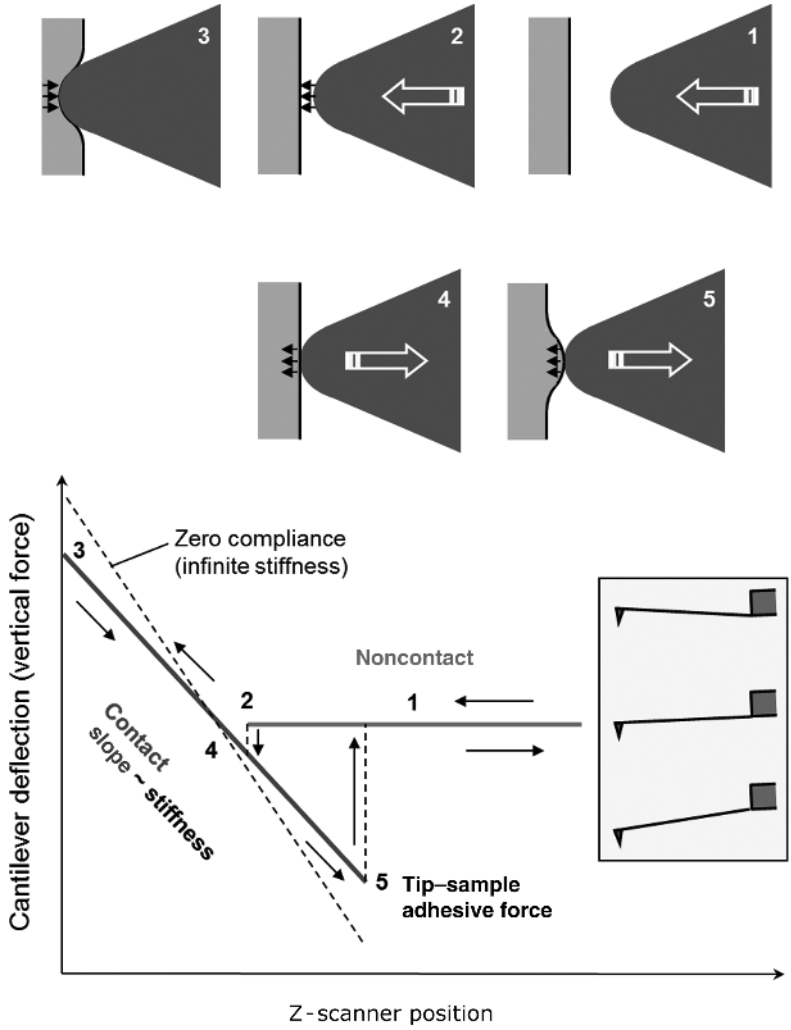

FIGURE 1.5 Tip–sample illustrations corresponding to select locations in a schematic force-curve cycle. (1) Tip and sample far enough apart that the interaction force is zero. (2) Tip close enough to sample so that attractive forces are felt and cause the tip to jump to contact (overcoming the resistance of the cantilever). (3) Maximum approach point with significant indentation into soft sample and repulsive forces acting on tip due to the sample deformation. (4) Return to state of zero indentation during retraction. (5) State of final contact just prior to the tip's jump from contact as the maximum pulling force of the cantilever exceeds the tip–sample adhesion. Inset depicts the directions of cantilever bending relative to the unbent stage (exaggerated).

measurement of stiffness and adhesion as seen in a *force curve* with accompanying illustrations of tip and sample. In Section 1.5, we treat force curves in greater detail, but for now, we consider only in the context of stiffness and adhesion images collected in a mode known by at least two commercial names: *pulsed force mode* and *peak force tapping*. (This is described in greater detail in Section 6.5.) During approach or retraction of the *Z* scanner to bring tip and sample together and then move them back apart at a given pixel location, one can render the *contact slope* as a datum of qualitative material stiffness. (Quantitative stiffness requires comparing this slope to the zero-compliance slope as approximated on a very rigid sample, the dashed diagonal line in Figure 1.5.) One commonly measures tip–sample adhesion as the maximum pulling force sensed upon retracting the tip from the surface with the *Z* scanner [6]. These measurements can be readily calibrated; the *Z*-scanner movement is quantified by imaging known height changes atop calibration gratings and the vertical cantilever bending is calibrated to equal the *Z*-scanner movement on a rigid sample (Chapter 3). This is converted to cantilever spring force by multiplying by the cantilever spring constant. Height in this mode can be gauged from the *Z*-scanner position at the turnaround point at maximum force (an operator-specified signal from the split photodiode).

Friction during continuous sliding contact is semiquantified as the change of lateral force signal upon reversing the lateral sliding direction, as seen in a *friction loop*. This is depicted in Figure 1.6 for two cases: relatively low and high applied (loading) forces. The latter is controlled by the value of cantilever bending maintained during lateral scanning, as can be selected during force-curve viewing. The measurement of the height of the friction loop removes the difficulty of measuring the *true zero* of the lateral quad photodiode signal and further removes most topography-derived contributions to lateral force as well as other artifacts that are independent of lateral scanning direction, as discussed in Chapter 7 (wherein procedures for friction force calibration are also described). The heights of friction loops on different surface domains—that is, the relative amounts of hysteresis—provide ratios of friction force, meaning quantitative materials contrast.

In the following, we consider examples of stiffness and adhesion imaging (Figure 1.7) and friction imaging (Figure 1.8). These cases are chosen to demonstrate not only the differentiation of similar materials but also the identification of chemical changes and differences in crystalline defect concentrations. Thus, these nontrivial examples illustrate the sensitivity of AFM as an analytical tool.

The images in Figure 1.7a and b are simultaneously acquired topography and stiffness for a blend of two chemically similar polymers—poly(butyl methacrylate) (PBMA) and poly(lauryl methacrylate) (PLMA)—that nonetheless dramatically differ in stiffness, PLMA being soft and rubbery and PBMA being relatively rigid and *glassy* (an amorphous solid state) [10]. Moreover, the right side of each image contains the as-prepared material and the left side the same material *after exposure to a 2.0-MeV helium ion beam* (used in Rutherford backscattering spectrometry) that preferentially depletes hydrogen and oxygen, leaving a carbonized (“burnt”) material. The topography contains a *reduced height* of about 600 nm from beam exposure at left due to the loss of atoms; the stiffness reveals a *lack of contrast* in

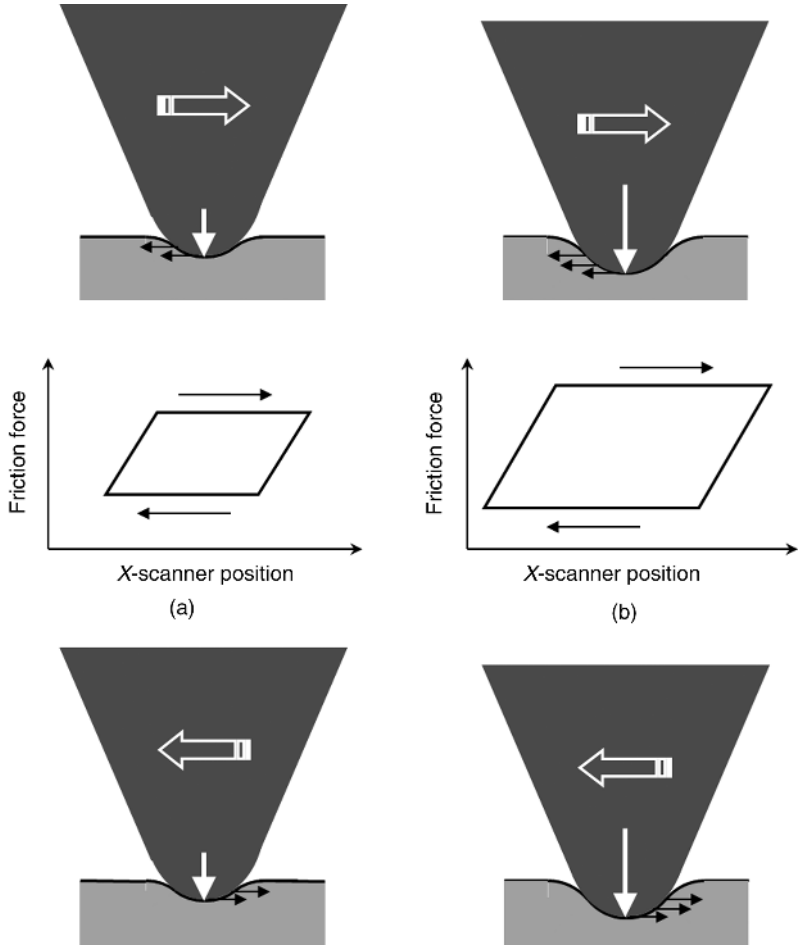

FIGURE 1.6 Friction loops and associated tip–sample illustrations for two cases of frictional imaging, (a) low and (b) high applied vertical force via different amounts of upward cantilever bending maintained as the tip slides over the surface.

the exposed region, whereas the as-prepared material at right contains soft (dark) and rigid (bright) domains, the phase-segregated polymer blend. The soft domains include a few large circles that correlate with circular dips or "craters" in topography; yet, many of the circular topographic features do not exhibit softness. There are also much smaller, soft circular domains.

But touching can be subtle indeed. The adhesion or pulling force needed to separate tip from sample is displayed in Figure 1.7c. Darker corresponds to lower adhesion. Here, we find a richer and subtler sensitivity to material differences at the surface. Most of the soft circular domains, but not all, exhibit lower adhesion—counterintuitively less "sticky", notably three large circular domains residing at the

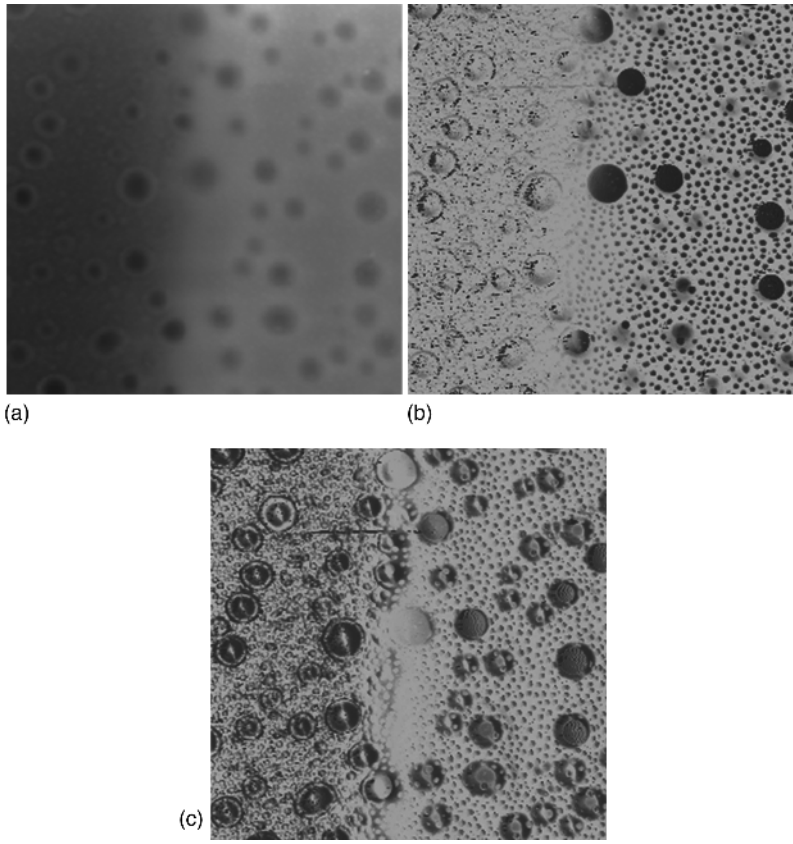

FIGURE 1.7 (a) Height, (b) stiffness, and (c) tip–sample adhesion images of a 75:25 blend film of PBMA and PLMA (spin coated onto a silicon wafer), 40×40 μm. The left portion of the imaged region had been modified by exposure to a 2-MeV beam of He ions.

boundary of the ion-beam-modified and unmodified regions. Moreover, there are many low-adhesion circular domains that do not seem to be soft. Even in the ion-beam-modified left side of the adhesion image, there are intriguing variations in tip–sample adhesion with little to no corresponding differences seen in the stiffness image.

All of these variations on materials contrast may seem bewildering for a seemingly simple, two-component system. Indeed, the complexity of Figure 1.7 is an example of what one often finds upon first viewing a property-sensitive image of a multicomponent sample: no shortage of contrast! In analytical science, a first goal is to measure differences. Then we have the potential to learn something. Sorting out what it all means, quantitatively and at a fundamental level, is always a remaining challenge. Some may balk at property-sensitive AFM imaging for this reason, while for many this challenge is the fun part! But our strongest motivation is the potential

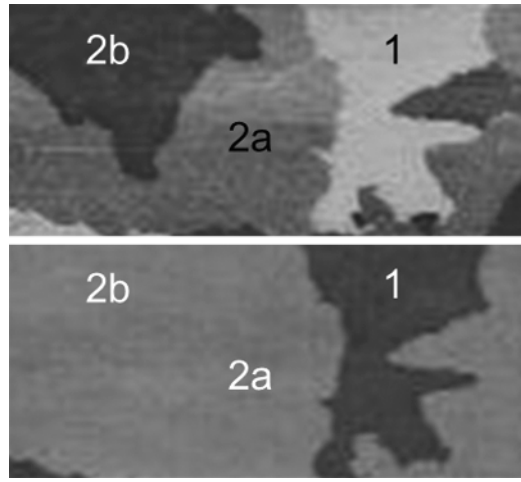

FIGURE 1.8 Ultrathin film (1.75 monolayers) of pentacene grown on an oxidized silicon surface, 7 μm across. Bottom image is topography of mostly second layer, partial first layer; top is simultaneously acquired friction force image.

payoff. From a utility standpoint, even qualitative and empirical findings that, say, correlate with material performance in technological applications can be very useful. In some cases, qualitative information obtained via material contrasting modes may be more important than quantitative topographic information.

Indeed, in some cases, topographic images tell us practically nothing, whereas the tip–sample interaction is astonishingly revealing. The magnitude of the sliding friction force can be exceedingly sensitive to *disorder* in crystalline organic systems as further discussed in Chapter 7. Our second example, in Figure 1.8, is a two-molecular layer film of pentacene, a molecule valued for its semiconductor properties and potential use in flexible electronic circuitry. The bottom topographic image, collected under continuous sliding contact, contains two shades corresponding to the surface heights of the first (dark) and second (light) layers, each about 2 nm thick. The top image displays the corresponding friction force and contains *three* shades, the brightest (highest friction force) measured atop the first layer, while both intermediate and low values are found *within the second layer*. The intermediate shade 2a, the higher friction within the second layer, corresponds to domains known to contain a higher amount of disorder in the form of *line dislocations*: flaws in the orderly packing of molecules into a 2D periodic array that result from stress, in turn, derived from a crystalline structure that is incommensurate with underlying crystal grains [11–13]. Understanding the fundamental, molecular-scale mechanisms of friction is a goal of the *nanotribology* research community [9]. But this example demonstrates how AFM can be highly useful even in the absence of first-principles understandings of *contrast mechanisms* (detailed identification of the kinds of molecular motion activated by the passing AFM tip).

1.3 MODIFYING A SURFACE WITH A TIP

Shear forces also can be used to "tear up" a material. A simple, practical use of this "abrasive" scanning is the analysis of multilayered films. Provided that the top layer is not too difficult to disrupt with the tip and the substrate or underlayer relatively impervious to this same scanning tip, the ability to expose the substrate or underlayer results [14]. One case is a polyvinyl alcohol (PVA) [15] film that can contain a discontinuous skin of highly crystalline and brittle polymer. It is quite easy to fracture or disrupt the skin and expose a more amorphous underlayer. An example is shown in Figure 1.9, where a subregion previously had been cleared down to the underlayer by scanning at an elevated applied force (i.e., by maintaining a greater upward bend of the cantilever). The larger region in Figure 1.9 was then imaged at a light force where further tearing did not result. The altered box is evident not only in the topography image at left but also in the corresponding friction force image at right. The friction also suggests that some ill-defined surface mixture of the two components has not resulted; the level of friction within the cleared region is equal to the level of friction found in the initial exposed underlayer at left. (Intermediate values are indeed found within the lip of material piled at the periphery of the cleared region).

One may wonder how well these scanning conditions, abrasive versus nonabrasive, can be controlled via the applied loading force. We have already mentioned in Section 1.2 that the magnitude and sign of force can be measured in force curves because the zero of force is measurable. The operator may thereby specify the value of force to be *maintained during imaging*, what we call the *setpoint*. Indeed, the operator may vary this setpoint and, thus, the applied force through different values and measure how the friction force changes. Even negative forces can be applied, which means pulling on the tip, with the cantilever bent down like a

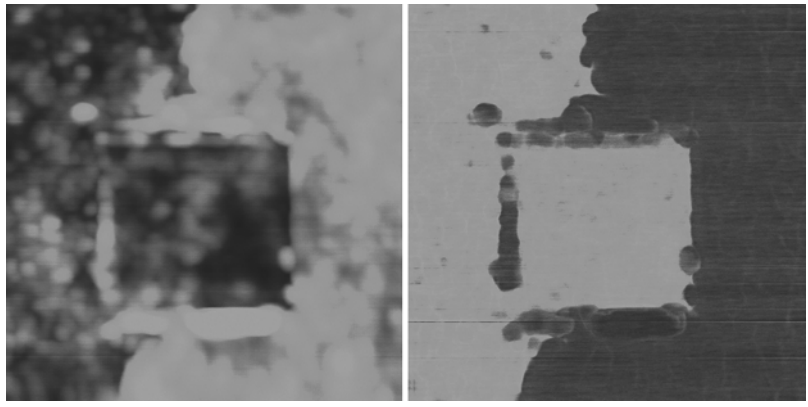

FIGURE 1.9 Topography (left) and friction force (right) images (1×1 μm) of PVA following abrasive scanning of a 500×500-nm subregion. The low-friction, highly crystalline topmost component is selectively disrupted.

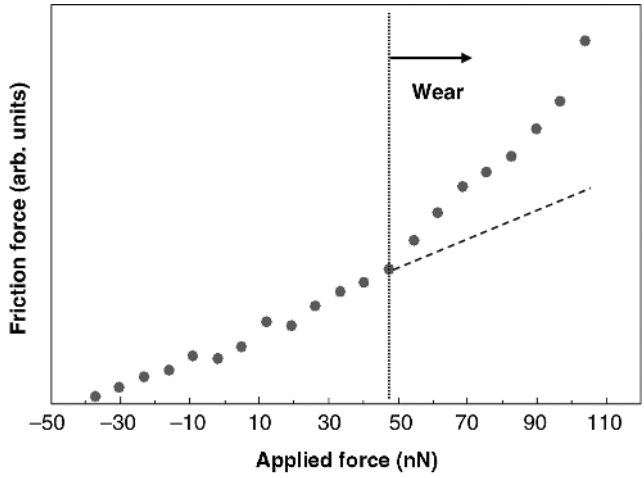

FIGURE 1.10 Friction force versus applied loading force atop a highly crystalline skin layer on a dry gelatin film.

stretched spring. In this case, contact is maintained by an even stronger adhesion force that pulls the tip in the opposite direction. We will discuss the analysis of quantitative friction–load data in Chapter 7. For the purposes here, one wishes to identify the onset of abrasion. This is typically seen as an increase of the *slope* of friction versus applied force, as shown in Figure 1.10 for the case of a (dry) gelatin film very similar to the PVA film examined in Figure 1.9, in which it contains a highly crystalline skin layer [14]. (Gelatin is a polypeptide derived from the protein collagen.) Thus, one can assign the initial low slope as intrinsic to friction in the absence of wear and friction forces above this extrapolated trend as due to wear processes.

This methodology has found utility in the biological as well as synthetic material realms. One example is a method to quantify cohesive strength of biofilms, specifically the extracellular polymer substances (proteins, polysaccharides) that serve as a "glue" to bind together a matrix containing bacterial cells, in the case of wastewater-treatment biofilms (Figure 1.11) [4]. *Cohesion* in and *adhesion* of biofilms is of great significance to many technological applications, whether this mechanical coherence is desirable, in the case of wastewater treatment, or undesirable, in the case of biofouling of surfaces that are preferred to remain clean. With successive AFM raster scans at relatively high loading forces, a gradual excavation of a hydrated biofilm matrix can take place (at 90% relative humidity), whereby chain molecules are disentangled and displaced by shear forces. During the course of this multi-raster scan treatment, one can reduce the loading (vertical) force to avoid abrasion, zoom out and acquire topographic images to assess the previous excavation process as done in Figure 1.9 (right image). Comparisons with an initial image of the pristine surface (Figure 1.9, left image) can be used to quantify the abraded surface. In particular, one can compute the volume of material

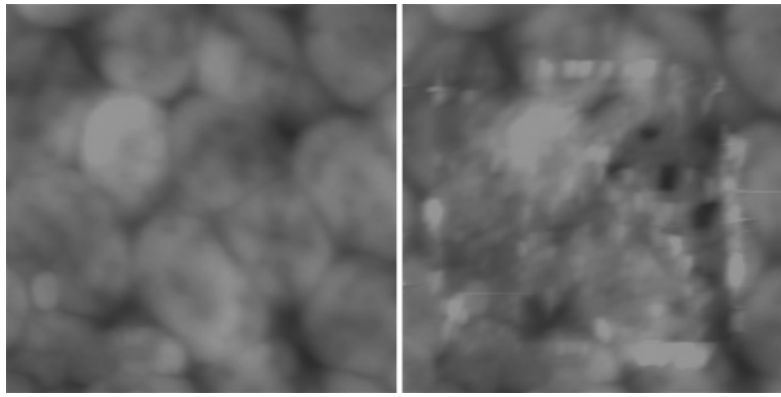

FIGURE 1.11 Topographic images ($3.7 \times 3.7\,\mu$m) of a wastewater treatment biofilm before (left) and after (right) AFM scanning at a destructive force within a square subregion ($2.5 \times 2.5\,\mu$m).

displaced by abrasive scanning. It is also possible to analyze the total friction force versus load to identify the fraction of frictional energy transfer that is responsible for abrading the biofilm, by extrapolating and subtracting the low-slope friction force that is unrelated to wear as suggested in Figure 1.10. By integrating the extra friction force due to wear over multiple raster scans, an aggregate frictional energy of wear can be measured. This energy, divided by the volume of film displaced, is then a measure of cohesive energy density [4], an intrinsic and exceedingly difficult property to determine by any method.

In addition to wear, many kinds of phenomena may be induced or catalyzed by tip–sample interaction. For example, it is well established that in air, *capillary transport* can take place, whereby molecules are transferred from tip to sample or sample to tip through a capillary *nanomeniscus* that forms at the tip–sample contact zone (Chapter 6) [16]. Even local oxidation of the surface can be carefully produced by an applied voltage bias between tip and sample under controlled humidity (to control the size of the meniscus). Many of these processes happen very rapidly. Indeed, just making a first contact of tip to sample can produce dramatic effects. In Figure 1.12, the initial touch of a freshly prepared gelatin film induced outward deformation ("doming") that extended many micrometers radially from the touch point (top-left image), together with a dramatic change in properties of this deformed region such as frictional response (top-right image). The presence and extent of this phenomenon is strongly dependent on film *age*. For gelatin, this means the *extent of a physical cross-linking network* as driven by collagen *renaturation*. Collagen is a connective protein (here extracted from mammal bone) that forms *triple-helical conformations* (shapes or structural arrangements). When chemically processed to form gelatin, these triple helices are "unwound" to isolate the individual molecules, but with passing time, triple helices reform as driven by the intrinsic biochemistry (hydrogen bonding of units in regular locations along the

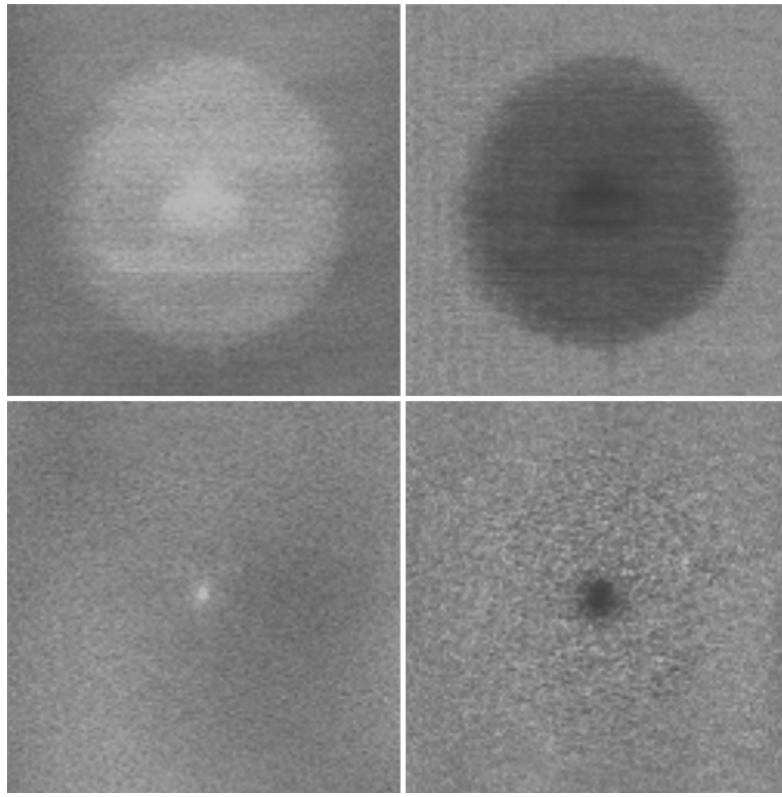

FIGURE 1.12 Height (left) and friction force (right) images ($10 \times 10\,\mu m$) of a (dry) gelatin film following approach and contact of tip to the center of the circular regions. Freshly prepared (top) and 1-week-old (bottom) films.

polypeptide chains). This produces *physical cross-links* that hold the polymer matrix together [17]. As the number of these cross-links increases, so does the stiffness of the matrix. Thus, an attractive force produces a doming of much smaller spatial extent as the film stiffens with age. After a week of aging, the touching of the same tip to surface produces an effect that is an order of magnitude smaller in spatial extent as seen in the bottom images of Figure 1.12 [18].

1.4 DYNAMIC (OR "AC" OR "TAPPING") MODES: DELICATE IMAGING WITH PROPERTY SENSITIVITY

When working with soft synthetic or biomaterials, or structures that weakly cohere or weakly adhere to substrate, one often discovers that the abrasion demonstrated in the previous section *cannot be avoided*, no matter how lightly one contacts the surface. A sliding tip, in the presence of tip–sample adhesion, may generate stress that

exceeds a *yield point*, damaging the material under study. Multiple strokes by the tip, given a particular stroking direction, result in displacements that do not "relax away." Repeated scans show an additive effect [19]. In many cases, there is no gross tearing of material, rather, a subtler transformation of surface topography. In some cases, *repeated raster scanning is required to unambiguously identify these effects* and, thereby, assess whether the observed topography is "true." In the process, one can sometimes discover fascinating behavior. For example, on glassy polymers, one can observe the formation of *periodic ripples* perpendicular to the fast-scan axis of the raster pattern during repeated scanning. Systematic studies have unveiled quantitative relationships between geometric characteristics of the ripples—such as periodicity and angle of orientation—and fundamental thermokinetic responses of the polymer (a subtopic of Chapter 7) [19–21]. Indeed, this suggests the *usefulness* of scan-induced patterning of thin polymer films to gauge molecular mobility, especially those motions pertinent to tribology.

Returning to the goal of obtaining a "nonperturbative" image, of avoiding the preceding phenomena, what should one do? Empirically, it was learned in the first years of AFM that the biggest problem is indeed shear forces. (It is not too difficult to imagine that the sliding tip depicted in Figure 1.6b might tear the highly stressed material!) Thus, a very brief and purely vertical touch of tip to surface, with the tip remaining *off the surface most of the time* while scanning the surface, is key to avoiding or minimizing many of the above problems. The general term for such an imaging scheme is *intermittent contact*. There is more than one way to implement intermittent contact, different modes of operation. In Section 1.2, we showed images acquired with high-speed force-curve mapping [22], which uses the *Z* scanner to approach and touch tip to surface then retract, as few as one touch per pixel in the image. This is actually a rather less-known method and will be discussed in more detail in Chapter 6.

A much more common implementation of intermittent contact is called "tapping mode" by most users (originally, a vendor's trademark for a particular implementation) that also goes by the names dynamic, AC, and vibrating mode, or in some cases, noncontact AFM as will be discussed [23]. This scheme indeed *vibrates the cantilever* at or near its fundamental flexural *resonance frequency* such that many cycles of approach and retract occur per pixel location. Thus, a time-averaged *dynamic* interaction results. But this vertical cycle is not produced by the *Z* scanner; the vibrating cantilever does all the work. The *amplitude* of vertical tip oscillation must be sufficiently large to overcome adhesion between tip and surface. The amplitude also is commonly used to enable the tracking of surface topography, but with a number of caveats and potential pitfalls, as described in detail in Chapters 4 and 5. Tracking means that the *Z* scanner reactively displaces the distance between oscillating tip and sample to *keep the tip amplitude constant*, reduced from its amplitude when free of the surface. This is depicted in exaggerated form in Figure 1.13, for the case where the *Z* scanner is displacing the cantilever chip to accommodate changes in surface elevation (some instruments instead displace the sample vertically).

In Chapter 5, we also describe a property-sensitive imaging mode, known as "phase" imaging, which proceeds in parallel with topographic imaging in dynamic

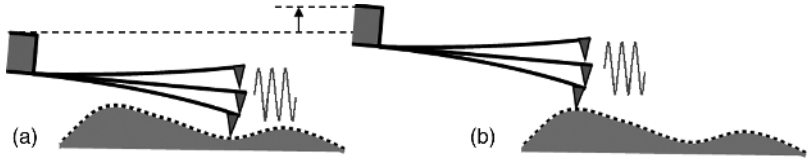

FIGURE 1.13 Exaggerated illustrations of topographic imaging via a vertically oscillating AFM cantilever/tip. An upward displacement of the chip to which the cantilever is attached allows the tip to maintain a constant oscillation amplitude whether (a) in a valley or (b) atop a hill. In actual operation, the oscillation amplitude is typically on the order of tens of nanometers, whereas the height of the tip is $\sim$10 μm.

AFM. We will see that this quantity can be more difficult to interpret than the adhesion, stiffness, and friction force images in the preceding sections, yet has proven exceedingly valuable to both fundamental and applied science and engineering. The "phase" is the *time shift between a sinusoidal driving signal that vibrates the base of the cantilever and the approximately sinusoidal motion of the tip end of the cantilever,* as the tip oscillates near and far from the sample surface. At first sight, it is not at all obvious why this measurement should provide materials contrast! Indeed of all AFM imaging modes, phase imaging is perhaps the most esoteric and almost certainly the most misinterpreted in published studies, conference presentations, and internal analytical reports. This is not because of a lack of published understandings. The core principles for understanding phase data were identified and published by the late 1990s in journals such as *Applied Physics Letters*, *Physical Review B*, and *Ultramicroscopy*. But with the massive growth in the presence of AFM's in laboratories of every sort, at institutions of every sort, coupled with the lack of formal training for most users of these systems, erroneous interpretations and poorly conceived instrument settings may often result.

There is firstly an intrinsic phase lag between the driving sine wave and the tip motion—which can be measured when the tip is oscillating far from the surface, out of *engagement* with sample—and secondly a phase shift resulting from tip–sample interaction. The latter shift results from the *modified resonant behavior of the cantilever* as discussed in Chapter 2 and later chapters. This phase shift provides materials contrast that may derive from *any and all portions of each approach–retract cycle*: whether the tip is sensing attractive forces far from contact (say due to a charged surface), or pushing into the surface, or breaking away, etc. Why use phase imaging if it *convolves* all of these different interactions? Well, it turns out that the extremely rapid, dynamic vertical oscillation can be controlled to provide an exquisitely *delicate* tip–sample interaction, even more so than other intermittent contact modes such as force-curve mapping. The most delicate case is a *noncontacting* oscillation; only attractive forces are sensed as the tip nears the surface because it does not get close enough to actually impact the surface, which would generate a repulsive force. This attractive interaction modifies the resonant behavior, as diagnosed in the phase shift; thus, the tip's oscillation amplitude decreases and enables the tracking of topography. Why this happens will become clearer in Chapter 2 and

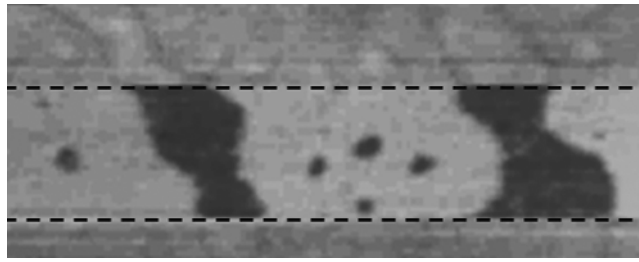

FIGURE 1.14 Topography image (1.4 μm wide) of an ultrathin polymer–surfactant complex film collected under two different parameter settings (inside and outside of dashed lines) in dynamic mode.

in further detail in later chapters. The very delicate interaction in this *attractive regime* allows difficult samples such as gels, nanoparticles weakly adhered to substrate, or even liquidy films to be imaged without tearing, plowing, puncturing, or other deleterious effects. Even some of the more robust, multicomponent materials—which can be imaged just fine with other modes—may be contrasted with *better resolution* in phase imaging because of the exceedingly brief (often <1 μs) and delicate interaction.

By varying imaging parameters, one can easily toggle from a "true topography" imaging regime to a regime with penetration of tip into sample, and often selective to material components as discussed in Chapters 4 and 5. An example of this phenomenon is the topography image in Figure 1.14, an ultrathin complex film (<10 nm) containing silicone oil (polydimethyl siloxane), the short-chain (~ 2 nm) *amphiphilic* molecule cetyl trimethyl ammonium chloride (i.e., one end being cationic and polar and thus water loving, the other oily and thus water hating), and probably bound water [24]. The horizontal dashed lines mark the point during raster scanning at which *instrument settings were altered* so as to switch from "true" topography (top and bottom) to "false" topography (middle), where the tip selectively penetrates nanoscale-thick liquidy domains to reach near the solid mica substrate a few nanometers below. The operational strategies for exploring such behaviors are discussed in Chapter 5.

So far we have not emphasized nanometer-scale lateral resolution. But AFM tips are sharp enough, and the brief tip–sample interaction is delicate enough, to enable a touching zone that is only ~ 1 nm across. This takes us into a regime of resolution that light microscopy cannot reach, far below the wavelength of visible light. One common example is indeed phase imaging, as described above, to discern *phase segregation* in *block copolymer* systems. Notice we are making use of two completely different meanings of the word "phase!" This of course adds to the confusion. Phase segregation refers to the tendency of certain substances to separate from one another, such as oil and water, provided thermal motion and time. Thus, one obtains domains rich in one type of molecule or another. Block copolymers are long-chain molecules containing long "blocks" of one homopolymer or another. That is, each long block contains repeated "mers" of the same chemistry, one polymer.

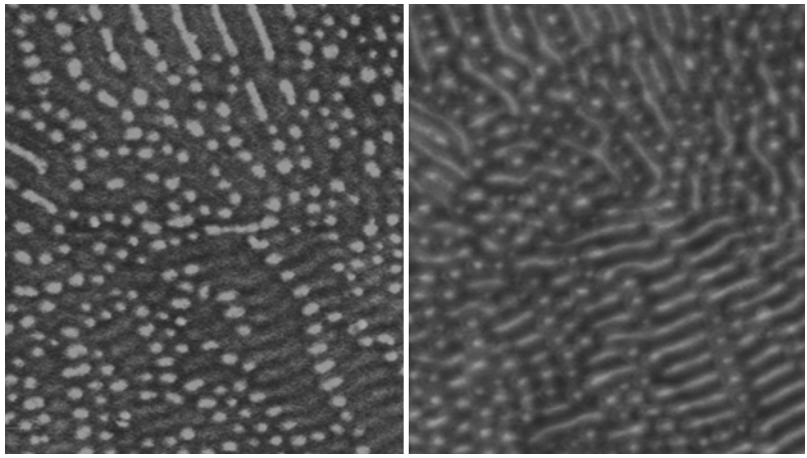

FIGURE 1.15 Dynamic-mode phase images (1 μm across) of a thick poly(styrene–isobutylene) triblock copolymer coating acquired using different imaging parameters to achieve different depth sensitivities.

Our example is an ABA block copolymer, meaning each long-chain molecule has an A block of polymer constituting the end chains, here polystyrene (PS), whereas the middle of each molecule is a B block of a different polymer, here polyisobutylene (PIB). Solid PS by itself is a rigid and glassy polymer, and PIB is soft and rubbery. The total length of the two PS blocks is about one-fourth of each chain molecule. The two phase images in Figure 1.15—here referring to the measured shift between two sine waves, driving and response—reveal phase-segregated PS and PIB domains, bright and dark, respectively—here referring to segregated materials on the ~50 nm scale. This means that like blocks from different chain molecules tend to bunch together to create PS-rich or PIB-rich domains. The lengths of the block chains result in 50-nm domains. Thus, longer molecules with longer blocks would produce larger than 50-nm domains, and shorter would produce smaller domains. The shape of the domains relates to the relative size of A and B; for our case, the tendency is for cylinders of PS to form in a matrix of PIB. An annealing step, exposing the polymer to solvent vapor for many hours, results in the orientation of cylinders either perpendicular or parallel to the surface, a more thermodynamically favored state [25].

The images in Figure 1.15 look similar because they correspond to the same surface region; yet they are different. The left image was acquired with a "light touch" and is thus "sharper." Moreover, it contains three levels of contrast as compared to two in the right image acquired under "pounding" conditions. This example illustrates how the exquisite sensitivity enables not only nanoscale lateral resolution (X–Y) but also vertical resolution (Z). If imaging parameters are selected to produce an extremely delicate touch—the case of the left image—then one can perceive the difference between PS at the surface (bright) or 1–2 nm below a "skin" of PIB

(intermediate tint). The latter tends to segregate to the surface–air interface due to its lower surface energy [26]. Selecting imaging parameters to produce a stronger push into the surface—the right image—makes the tip "feel" the stiffer PS equally, whether at the surface or under 1–2 nm of soft PIB. The result is a single level of response for PS (brighter) instead of two levels. (We will discuss these operational parameters in Chapter 5.) Also, the boundaries between regions are more blurred in the right image; by pushing deeper into the polymer, a larger *contact area* between tip and sample is formed, meaning coarser image resolution.

1.5 FORCE CURVES PLUS MAPPING IN LIQUID

It is not only imaging that is enabled by nanoscale force probing. The *distance dependence of force* between tip and sample, acquired in a force curve,[8] can elucidate many physical traits of materials and biomolecules. Note that this differs from the *time-integrated* sensitivity of dynamic AFM, the preceding section, to these same distance-dependent forces. (In that case a variety of forces—including attractive and repulsive, short and long range—are convolved into one number, the phase shift.) Examples include the strength of interfacial attraction or repulsion, molecular binding or unbinding, rigidity and viscous resistance to tip motion, as well as fundamental studies of these phenomena via rate and/or temperature dependences [7]. Although typically acquired at a single-point location within the *X–Y* range of the scanner, force curves can also be collected using *X–Y-mapping routines*, meaning a 3D domain or "data cube." The detailed algorithms for doing this differ among commercial AFM systems and go by commercial names such as *Force Volume* and *SPS Imaging* in addition to the already-mentioned *Pulsed Force Mode* and/or *Peak Force Tapping*. Moreover, the data can be analyzed within subregions of the explored domain, although commercial data-analysis routines remain somewhat limited at this writing. (Third-party software and public-domain routines exist for this purpose.)

The details of force-curve acquisition and data interpretation are discussed in Chapters 2, 3 and 6, and force-curve mapping also is discussed in Chapter 6. Here, we preview two examples in processed form. The three full-cycle (approach-retract) force curves in Figure 1.16a were acquired under deionized water immersion from three surface locations on a thin-film system: (1) a silanized glass substrate, cleared by abrasive AFM scanning (at elevated force), (2) surrounding lip of disrupted polyacrylamide film, and (3) undisturbed polymer (swelling ∼300%). This sample region was prepared for the purpose of measuring the water-swollen film thickness and analyzing the behavior of chain molecules in different conformational states. Conventional (sliding) contact-mode height images in water are shown in Figure 1.16b and c, as (a) color-mapped height to examine Z values and (b) differential height ($\delta Z/\delta X$) to enhance texture.

[8] Also called force–distance curves, force-displacement plots, force calibration plots, force spectroscopy, approach-retract curves, or force profiles.

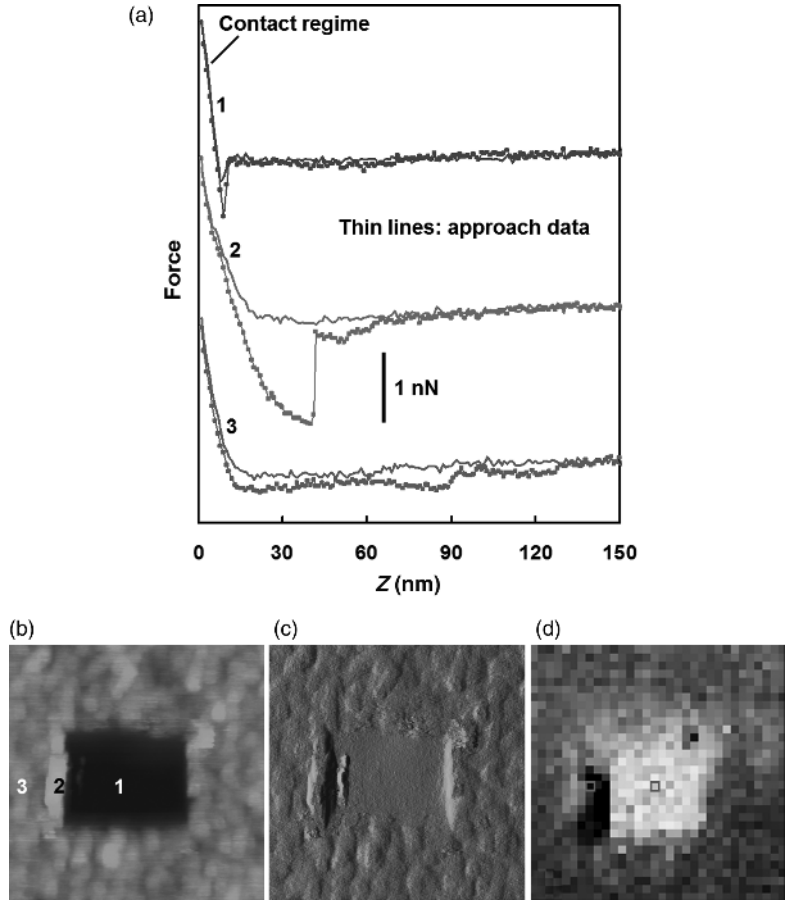

FIGURE 1.16 (a) Raw force curves obtained in deionized water at three characteristically different locations on a scan-abraded polyacrylamide film in water as imaged over 1.5×1.5 μm in (b)–(d). (b) Contact-mode height image of film and exposed glass substrate collected in conventional (sliding) contact mode. (c) Differential height image (slope of surface along horizontal) to highlight texture. (d) Stiffness mapping, the steepness of each force curve in the contact regime near the turnaround point. Open squares denote the locations of the force curves in (a).

There are several interesting features contained in the three force curves. During approach from right to left, short-range attractive forces (a steep downward dip) are felt above the bare glass within a 5-nm distance, but not either case of polymer. Upon "contact," the steepness of growing positive force (resistance) reflects mechanical stiffness that differs among locations. Figure 1.16d contains a qualitative stiffness mapping generated with a custom software algorithm [27], brighter being higher stiffness. The sites of the three force curves are denoted by corresponding open squares. The stiffest contact is obtained on the exposed glass

substrate, whereas the softest contact is on the disrupted polymer to the immediate left of the exposed substrate. During retraction, dramatic differences in tip–sample adhesion are visible, indeed very large variations in the size of the *hysteresis* or *irreversibility*. The hysteresis loop is particularly large at location 2 because of the polymer disrupted by abrasive scanning. Weak attractive forces are sensed to distances of ~100 nm on region 3, the undisturbed polymer, meaning long chain molecules remain attached to the tip, spanning the gap between the tip and the film.

Such rich and characteristic behaviors (further examined in Chapter 6) can be qualitatively or semiquantitatively probed by even novice AFM operators in a matter of minutes including setup time. Even a qualitative examination may provide sufficient answers to one's analytical questions. As with topographic imaging, however, AFM can tell us much more—with more effort—because of the *quantitative* nature of the measurements. In later chapters, we will delve into systematics as well as some important realities and caveats. But for the moment, let us look at one example in a little more detail: relatively short-range attraction between SiO_2 tip and a *silanized* (i.e., made *hydrophobic*) glass substrate. We see in Appendix 2 that the result of summing atomic or molecular dipole–dipole interactions between a spherical-ended model tip and a flat surface is in an *inverse-squared* distance dependence of attractive force, which becomes negligible beyond a few nanometers. We will also see that immersing in a liquid medium can add further complexities that are nevertheless open to quantitative and fundamental analysis. Figure 1.17 contains a force–distance relationship for a SiO_2 tip and a silanized

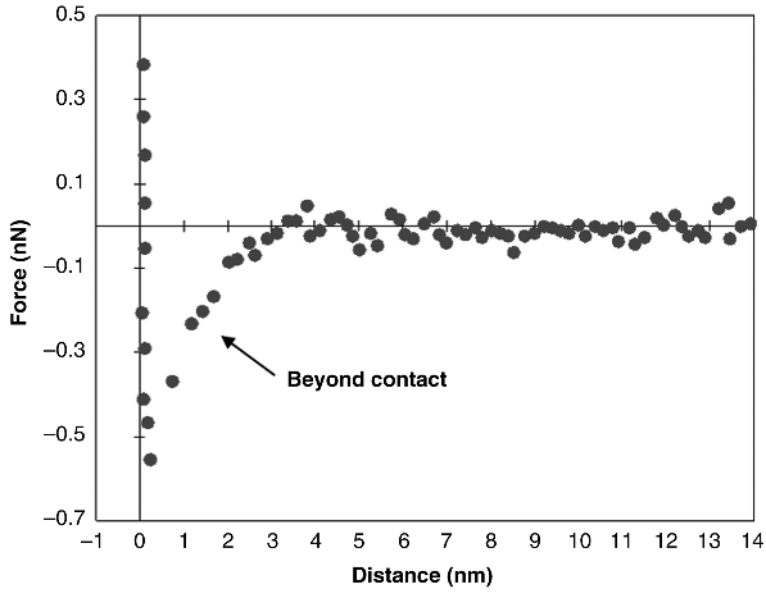

FIGURE 1.17 Force–distance relationship in water between a SiO_2 tip and a silanized SiO_2 surface.

SiO_2 surface immersed in deionized water, acquired at much higher data density along the distance scale than the top force curve in Figure 1. Moreover, this scale has been calibrated to account for both the *controlled* distance displacement of the *Z* scanner and the *uncontrolled* vertical bending of the cantilever (Chapter 3).

An important parameter in the theoretical expression describing the attraction between tip and sample beyond contact is the *Hamaker* constant, which relates to the mutual *polarizability* of pairs of interacting atoms. The dipole–dipole nature of forces responsible for this behavior on uncharged surfaces ensures a very short-range force compared to the *electrostatic* force between charged surfaces, or for that matter between a charged and uncharged surface. In Chapter 2, we will explore the world of intersurface forces in greater detail, including cases where the presence of more than one type of force results in both short- and long-range forces, even producing *nonmonotonic* (e.g., oscillatory) force–distance relationships, where the net force alternates between attractive and repulsive as a function of distance.

In-liquid surface force characterization can be made even more rigorous with control of *tip chemistry*. Most commonly, hydrophilic versus hydrophobic terminal chemistries have been prepared, primarily using alkyl thiolate self-assembled monolayers attached to gold-coated tips. Using ionizable terminal groups, tip charge states can be selected by choice of pH or ionic concentration in solution, allowing the analyst to toggle between attractive and repulsive tip–sample interactions indicative of the local surface charge state. Thus, force–distance measurements have become a useful tool in the hands of analytical and surface chemists, revealing nanoscale variations. Indeed, biomolecules or biochemical functionalities also can be attached to the tip or, in some cases, placed at the end of a polymeric "tether" (e.g., polyethylene glycol (PEG)), to provide *stereochemical* freedom: the ability of the functional groups at the end of the tether to rapidly explore orientations and thereby bond to complementary stereochemical groups on a biological surface. This "fly fishing" mode then can be used to search for sites of *specific* biological adhesion such as those operative on cell surfaces (e.g., in ligand-receptor bonding). These sites usually require much a stronger pulling force by the AFM cantilever in order to separate the tip-attached group from the biofunctional group on the sample surface—probably involving relatively strong hydrogen bonding—and are thus differentiated from *nonspecific*, weaker interactions of purely dipole–dipole character (Chapter 2).

1.6 RATE, TEMPERATURE, AND HUMIDITY-DEPENDENT CHARACTERIZATION

From a scientific standpoint, AFM has matured into more than nanoviewer, nanomanipulator, or nanosensor of interfacial phenomena, fascinating and useful as these capabilities may be. The systematic variation of measurement rate and/or sample temperature can provide rigorous analyses of activated processes ranging from molecular motion (e.g., as manifest in the frictional properties of polymers [28,29]) to electronic transport (e.g., electronic conduction mechanisms in organic semiconductors) [30]. Thus, AFM can be used as a nanoscale dynamic mechanical

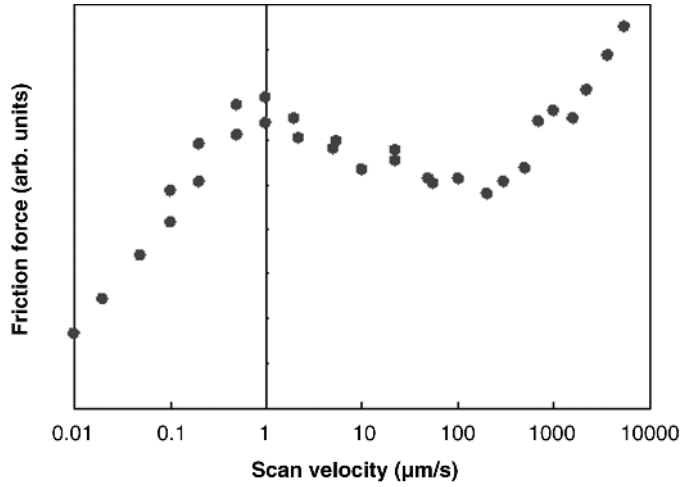

FIGURE 1.18 Scanning velocity dependence of friction force for a Si_3N_4 tip on a (dry) gelatin surface.

or thermal analyzer (DMTA) or rheometer [31], among other things, and ultimately as a tool for fundamental research in condensed-matter physics or physical chemistry. Here. we give three examples involving rate-dependent sliding friction, temperature-dependent stiffness and adhesion, and humidity-dependent phase imaging.

Figure 1.18 contains a graph of friction force versus tip scanning velocity, in micrometers per second ranging nearly *six decades of rate*—varied via a combination of scan size and scan frequency (lines per second)—on a gelatin film. A peak around 1 μm/s represents a dominant activated molecular motion—typically, rotational isomeric [32] or "turnstile" type—that tends to be in synchronization with, and thus excited by, the passing tip at a particular scanning velocity [33]. Another way to think of it is the characteristic time during which the passing tip interacts with the motional group. Different kinds of motion occur over very different time scales, as is well known from conventional *viscoelasticity* characterization [10]. Indeed, above 1000 μm/s, the friction force steeply increases again because another, much faster characteristic motion is preferentially excited. If our rate measurement window extended one or two decades higher, this peak would be resolved (friction force would again decrease). Such dissipative peaks, separated by several decades of rate, embody molecular motions of very different spatial extent, with longer range and *cooperative* motions (multiple synchronous activations) requiring more time, thus producing peaks at lower rates [10]. Thus, the scanning rate can be explored to bring out contrast in complex materials. For example, a polymeric material may contain local domains of heightened water content, increasing the activation of cooperative molecular motion, and thus the imaged friction force, at certain scanning rates [34]. We shall discuss such processes in greater detail in Chapter 7. This rate-dependent spectrum of activated motion can be relevant to all

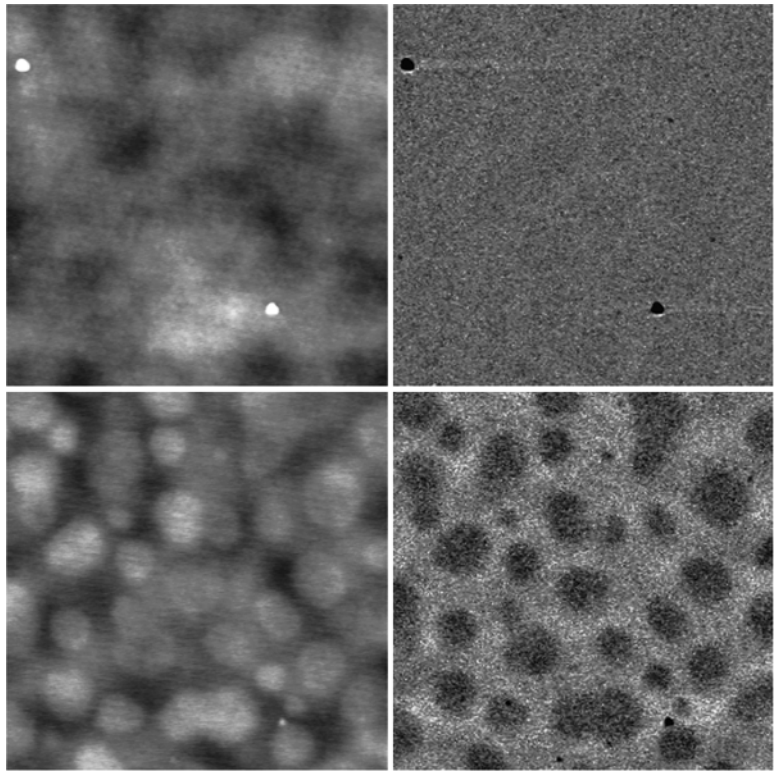

FIGURE 1.19 Rapid force-curve mapping AFM topography (left) and tip–sample adhesion (right) images 2.5 × 2.5 μm of a 50:50 blend of PMMA and PEMA at sample temperatures of 70°C (top) and 95°C (bottom).

sorts of polymeric technologies as well as the processing stages during manufacturing [35]. The characteristic rates also may be *modified by confinement to molecular-scale dimensions*, say in thin films or nanocomposites. Thus, one needs a tool such as AFM that can interrogate these behaviors down to the nanometer scale.

Our second example of this section, in Figure 1.19, is a blend of two methacrylate polymers that are glassy (rigid) at room temperature: polymethyl methacrylate (PMMA) and polyethyl methacrylate (PEMA). We compare topographic and pull-off force ("adhesion") images (left/right) collected at two sample temperatures, 70°C and 95°C (top/bottom). At 70°C, there are indistinct hills and valleys seen in height contrast (apart from two particulate contaminants) and essentially no adhesion contrast. At 95°C, there appear to be additional islands in height with distinct edges, and correspondingly dark adhesion domains (less sticky). The reason, at 95°C, the PEMA has softened because it is now rubbery instead of glassy—we have exceeded its *glass-to-rubber transition temperature*, T_g—whereas the PMMA has remained rigid (its glass–rubber transition being well above 100°C). Upon softening, the tip pushes farther into the PEMA by about 3 nm to achieve the force

setpoint that is being maintained constant via feedback. The additional Z displacement needed to reach this point is contained in the topography image—being rendered as a lower elevation—even though it is not really topography (as discussed in Chapter 4). The onset of adhesion contrast results from the phenomenon known as *adhesion hysteresis* (Chapter 6) that includes a *memory* of the tip–sample contact area. Upon reversal, the pulling force required to break contact relates back to the tip–sample contact area reached at the maximum pushing force, greater on the softer polymer. A more continuous measurement of penetration and/or adhesion versus slowly ramped temperature can be used to precisely measure the glass-to-rubber transition temperature [36]. As with rate dependence, the T_g's of many polymeric materials are important to myriad applications as well as behavior during processing, and can be strongly affected by nanoscale confinement.

Our third example of this section, in Figure 1.20, is a phase image of a block copolymer coating of interest for its biodegradability. It is imaged in dynamic AFM

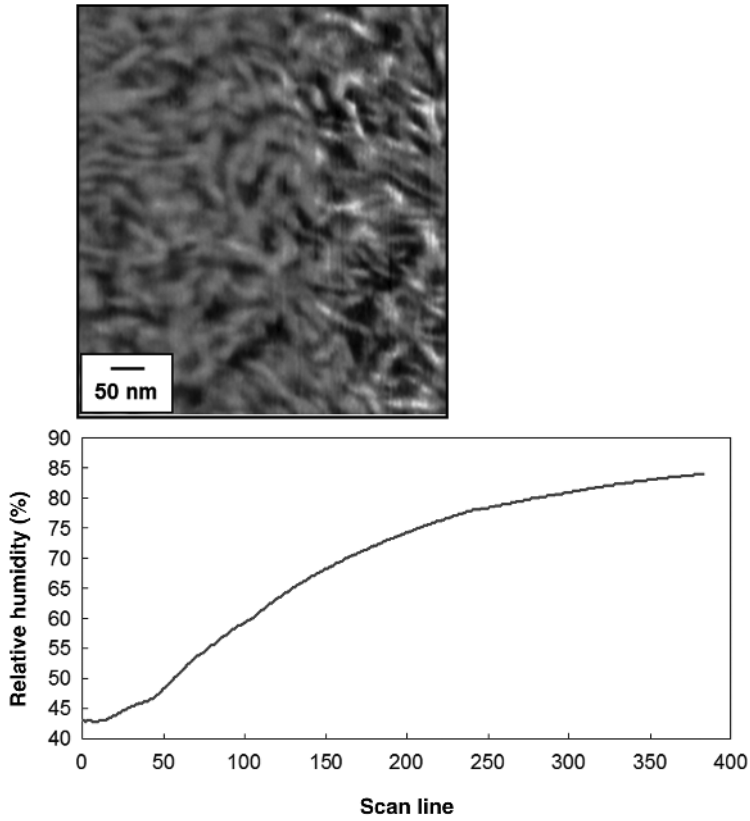

FIGURE 1.20 Phase image of PolyActive, a block copolymer of PBT and PEG, during the ramping of relative humidity from 43% at the beginning of the image at the left end to 77% at the end of the image at right.

under a continuous ramping of humidity from low to high as the image was collected from left to right (i.e., rotated by 90° from the usual orientation). This polymer contains both polar and thus hydrophilic (water absorbing) and oily and thus hydrophobic (water repelling) blocks; the latter tend to crystallize, further lessening the potential for water molecules to penetrate. Specifically, the hydrophilic blocks are (glassy) PEG and the hydrophobic blocks are polybutylene terephthalate (PBT). At low humidity, at which comparably little water has been absorbed into the hydrophilic blocks, we find only minor phase contrast. As the humidity reading rises above ∼65%, strong phase contrast results (an effect that is reversible with humidity decrease). This image was acquired under settings that produce strong intermittent contact and thus the phase contrast derives primarily from mechanical differences. The water-swollen PEG comprises a soft matrix within which rod-like domains of stiffer, unswollen PBT produce brighter phase. A more detailed and quantitative discussion of phase is the principal subject of Chapter 5.

1.7 LONG-RANGE FORCE IMAGING MODES

In several chapters, we will consider attractive forces sensed from distances ranging from nanometers to micrometers, meaning not only dipole–dipole forces but also electrostatic forces. These forces may be very weak, requiring AC (dynamic) modes to detect and quantify with good signal-to-noise ratio. We will see that the same type of "phase" measurement discussed in Section 1.4, and via this phase, the resonance frequency of the cantilever, can allow one to measure the *gradient* of force versus distance (as discussed in Chapters 2 and 9), which, in turn, reflects the strength of attraction between tip and sample. But how do you image phase or cantilever resonance frequency at well-defined distances of tens or hundreds of nanometers, yet be sure that a variation in surface height, and thereby tip–sample distance, is not the source of contrast? The most common approach, discussed further in Chapter 9, is a tracking procedure called *interleave*, illustrated in exaggerated form in Figure 1.21. This works by first collecting a single line of height data $Z(X)$ in dynamic mode, then repeating this same scan trajectory but at a distance of typically nanometers or tens of nanometers, relative to the topographic trace measured in the first pass, by offsetting $Z(X)$ by a fixed amount, $Z(X) + Z_0$. Certain

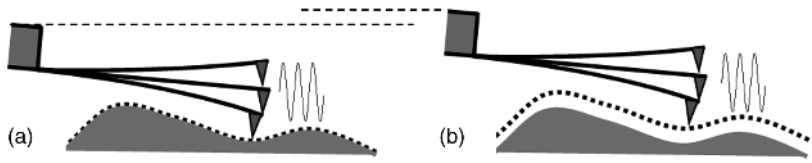

FIGURE 1.21 Exaggerated illustration of (a) a first scan to acquire topography and (b) a second interleave scan at a fixed mean displacement from the surface while phase or frequency shift are measured. The oscillation amplitude and vertical displacement are typically on the order of tens of nanometers, whereas the height of the tip is ∼10 μm.

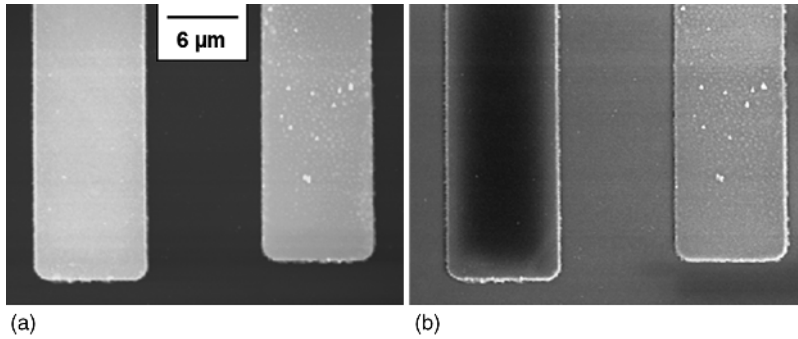

FIGURE 1.22 (a) Height and (b) phase images of strips of ∼50-nm tall aluminum (left) and gold (right) on a silicon substrate. The phase image was collected during the interleave scan where the oscillating tip was pulled an extra 50-nm away from the surface and the sample biased by 3 V. Darker phase corresponds to stronger attractive force.

parameters may be altered for the second pass, including the application of a voltage bias between tip and sample to detect electrostatic differences (e.g., charging). Even magnetic differences can be probed at this relatively large distance by employing a tip with a magnetized coating. These modes are usually called electrostatic (or electric) force microscopy (EFM) and magnetic force microscopy.

Figure 1.22 exemplifies the sensitivity of interleave-based phase imaging in EFM, with tip and sample displaced an extra 50 nm apart while the sample is biased by 3 V. The high (bright) domains in the height image (a) are metal strips, aluminum and gold, which were lithographically created on silicon, as is common in microelectronics. In the phase image (b), we see that the strength of attractive forces sensed at such a "large" distance (compared to the range of dipole–dipole forces) is nevertheless different for each of the three materials. Darker phase corresponds to stronger long-range attraction as discussed in detail in Chapter 9. Variability within each metal region derives in part from surface contamination left over from the lithographic growth process.

Even under zero bias there can be differences in the strength of long-range forces sensed by the tip due to intrinsically different *surface potentials*. On metals, this corresponds to different *work functions*, the energy needed to take an electron from the *Fermi level*—the highest-energy occupied electronic state (which can be excited slightly higher to produced electrical conduction)—to the *vacuum level*, just enough energy to escape the solid. A related interleave-based imaging mode actually maps surface potential by adding a variable voltage bias to tip or sample so as to negate the intrinsic surface potential difference of tip and sample, thereby "nulling" the force. The variation of applied bias with position across the surface, as needed to null the force, provides an image of surface potential variations. This mode is most commonly called Kelvin-probe or just Kelvin force microscopy (also, scanning surface potential microscopy) and is further detailed in Chapter 9.

In summary, we see that electromagnetic phenomena can be imaged with AFM. One approach uses interleave to enable the measurement of "long-range" forces in

parallel with topographic imaging (the latter obtained via short-range forces). Figure 1.22 demonstrates that tip–sample distances can be carefully controlled down to the nanometer scale to enable the probing of both long- and short-range forces, even though the imaged region may be tens of micrometers in size, and using just one device, the *X–Y–Z* scanner under electronic feedback. The development of the first commercial AFMs *and* the further equipping with advanced scanning modalities such as interleave occurred within just a fraction of a decade. This was in part due to the already advanced scientific understanding and engineering know-how for *piezoelectric materials* and scanners made from them, as well as fast electronic feedback control. We will discuss these subsystems in greater detail in Chapters 3, 4 and 9.

1.8 PEDAGOGY OF CHAPTERS

The overview of Sections 1.1–1.7 is partly intended to help point the reader to the chapter or chapters of greatest interest or urgency. Overall, the chapters are pedagogically arranged by grounding the technique in the concepts of distance-dependent forces in Chapters 2 and 3. Chapter 2 explores the topic from the standpoint of physical phenomena, divorced from instrumentation realities. Chapter 3 then drills down into the methods by which the AFM instrumentation actually measures these distance-dependent forces, whether in their own right or as a means to enable topographic imaging. Given these capabilities, Chapter 4 covers the methodology of topographic imaging in both quasistatic (contact) and dynamic ("AC"/"tapping") modes, including numerous realities and caveats that the AFM user will want to understand so that artifacts are avoided, accuracies are not overstated, etc. Issues affecting the choice of tip or cantilever and imaging mode will be discussed in the process. Chapter 4 also clarifies the nature of topographic data as manipulated during postprocessing. Chapter 5 focuses on phase measurement and imaging—for both diagnostic and materials contrast reasons—in dynamic AFM, including several difficulties, caveats, and calibration issues as well as examples of the kinds of information obtained. Chapter 6 covers tip–sample adhesion including both solid–solid (tip–sample) and capillary adhesion forces. It further describes mapping methods that examine force–distance measurements (force-curve mapping) in the quasistatic sense (maintaining a balance between tip–sample force and cantilever-applied force), as well as the distance dependence of amplitude and phase within dynamic AFM. Chapter 7 covers lateral-force-derived methods within (continuous) contact modes. Chapter 8 describes common data postprocessing and analysis methods. Chapter 9 treats more advanced dynamic methods for probing long-range electromagnetic forces via interleave methods, as well as newer dynamic methods that examine higher vibrational modes of cantilevers, for probing both long- and short-range force responses.

The appendices are intended to augment and in some cases provide greater mathematical detail on topics treated in the chapters. Appendix 1 describes three spectral methods for cantilever spring constant calibration, an augmentation to the conceptually simpler calibration method of Section 3.7. Appendix 2 uses integral calculus to derive van der Waals force–distance expressions for various tip geometries as

discussed in Section 2.2. Appendix 3 uses power balance concepts and calculus to derive energy dissipation expressions useful to phase data interpretation, as discussed in Section 5.3. Appendix 4 provides an explicit geometric description of a capillary meniscus in the circular approximation, as discussed in Section 6.3.

REFERENCES

[1] Binnig, G., C.F. Quate, and C. Gerber, Atomic force microscope. *Phys. Rev. Lett.*, 1986, **56**(9): 930.

[2] Sarid, D., *Scanning Force Microscopy*. Revised ed., 1994, New York: Oxford University Press, p. 263.

[3] Haugstad, G., et al., Atomic force microscopy of AgBr crystals and adsorbed gelatin films. *Langmuir*, 1993, **9**(6): 1594–1600.

[4] Ahimou, F., et al., Biofilm cohesiveness measurement using a novel atomic force microscopy methodology. *Appl. Environ. Microbiol.*, 2007, **73**: 2897–2904.

[5] Zangwill, A., *Physics at Surfaces*. 1988, Cambridge: Cambridge University Press, p. 454.

[6] Drelich, J. and K.L. Mittal, eds. *Atomic Force Microscopy in Adhesion Studies*. 2005, Leiden-Boston: VSP.

[7] Bhushan, B., ed. *Springer Handbook of Nanotechnology*. 2nd ed., 2007, Berlin: Springer.

[8] Bhushan, B. and H. Fuchs, eds. *Applied scanning probe methods XII: Characterization*. Nanoscience and Technology, 2009, Berlin/Heidelberg: Springer.

[9] Gnecco, E. and E. Meyer, eds. *Fundamentals of friction and wear on the nanoscale*. Nanoscience and Technology, ed. P. Avouris, et al. 2007, Berlin: Springer-Verlag, p. 714.

[10] McCrum, N.G., B.E. Read, and G. Williams, *Anelastic and Dielectric Effects in Polymeric Solids*. 1967, London: Wiley.

[11] Puntambekar, K., et al., Structural and electrostatic complexity at a pentacene/insulator interface. *Adv. Funct. Mater.*, 2006, **16**: 879–884.

[12] Schwoerer, M. and H.C. Wolf, *Organic Molecular Solids*. 2007, Weinheim: Wiley-VCH Verlag, p. 438.

[13] Kalihari, V., et al., Observation of unusual homoepitaxy in ultrathin pentacene films and correlation with surface electrostatic potential. *Adv. Mater.*, 2009, **21**: 1–7.

[14] Haugstad, G., et al., Probing biopolymers with scanning force methods: Adsorption, structure, properties, and transformation of gelatin on mica. *Langmuir*, 1994, **10**: 4295–4306.

[15] Finch, C.A., *Polyvinyl Alcohol: Properties and Applications*. 1973, London: Wiley.

[16] Piner, R.D., et al., Dip pen nanolithography. *Science*, 1999, **283**: 661–663.

[17] Djabourov, M., Architecture of gelatin gels. *Contemp. Phys.*, 1988, **29**(3): 273–297.

[18] Haugstad, G., W.L. Gladfelter, and R.R. Jones, Scanning force microscopy characterization of viscoelastic deformations induced by precontact attraction in a low cross-link density gelatin film. *Langmuir*, 1998, **14**: 3944–3953.

[19] Schmidt, R.H., G. Haugstad, and W. Gladfelter, Scan-induced patterning in glassy polymer films: Using scanning force microscopy to study plastic deformation at the nanometer length scale. *Langmuir*, 2003, **19**: 898–909.

[20] Schmidt, R.H., G. Haugstad, and W.L. Gladfelter, Scan-induced patterning and the glass transition in polymer films: Temperature and rate dependence of plastic deformation at the nanometer scale. *Langmuir*, 2003, **19**: 10390.

[21] Schmidt, R.H., G. Haugstad, and W.L. Gladfelter, Correlation of nanowear patterns to viscoelastic response in a thin polystyrene melt. *Langmuir*, 1999, **15**(2): 317–321.

[22] Krotil, H.U., et al., Pulsed force mode: A new method for the investigation of surface properties. *Surf. Interface Anal.*, 1999, **27**(5–6): 336–340.

[23] Garcia, R. and R. Perez, Dynamic atomic force microscopy methods. *Surf. Sci. Rep.*, 2002, **47**: 197–301.

[24] Haugstad, G. and A. Avery. Probing the morphology and tribo-response of nanostructured fluid films for personal care applications, in Technical Proceedings of the 2005 NSTI Nanotechnology Conference and Trade Show. 2005, Anaheim, CA: Nano Science and Technology Institute.

[25] Lazzari, M., G. Lui, and S. Lecommandoux, eds. *Block Copolymers in Nanoscience*. 2006, Weinheim: Wiley-VCH.

[26] Karim, A. and S. Kumar, eds. *Polymer Surfaces, Interfaces and Thin Films*. 2000, Singapore: World Scientific Publishing, p. 294.

[27] Haugstad, G. Probing swelling and molecular conformation on polymeric coatings for biocompatibility, in 225th ACS National Meeting. 2003, New Orleans, LA: American Chemical Society.

[28] Hammerschmidt, J.A., G. Haugstad, and W.L. Gladfelter, Probing polymer viscoelastic relaxations with temperature controlled friction force microscopy. *Macromolecules*, 1999, **32**: 3360.

[29] Overney, R.M., et al., Glass and structural transitions measured at polymer surfaces on the nanoscale. *J. Therm. Anal. Cal.*, 2000, **59**: 205–225.

[30] Choi, S.H., B. Kim, and C.D. Frisbie, Electrical resistance of long conjugated molecular wires. *Science*, 2008, **320**(5882): 1482–1486.

[31] Aklonis, J.J. and W.J. MacKnight, *Introduction to Polymer Viscoelasticity*. 2nd ed., 1983, New York: Wiley, p. 295.

[32] Wade, L.G., *Organic Chemistry*. 2nd ed., 1991, Englewood Cliffs: Prentice-Hall, p. 1233.

[33] Hammerschmidt, J.A., et al., Polymer viscoelastic properties measured by friction force microscopy. *Macromolecules*, 1996, **29**(27): 8996–8998.

[34] Haugstad, G., et al., Probing biopolymer films with scanning force methods. *Mat. Res. Soc. Symp. Proc.*, 1995, **355**: 253–258.

[35] Ferry, J.D., *Viscoelastic Properties of Polymers*. 1980, New York: Wiley.

[36] Tsui, O.K.C., et al., Studying surface glass-to-rubber transition using atomic force microscopic adhesion measurements. *Macromolecules*, 2000, **33**: 4198–4204.